Computer Methods and Programs in Biomedicine 226 (2022) 107121

Contents lists available at ScienceDirect

Computer Methods and Programs in Biomedicine

journal homepage: www.elsevier.com/locate/cmpb

Cardiac cells stimulated with an axial current-like waveform reproduce electrophysiological properties of tissue fibers

Violeta Monasterio[a,*], Esther Pueyo[b,c], José Félix Rodríguez-Matas[d], Jesús Carro[a]

[a] Universidad San Jorge, Villanueva de Gállego, Spain
[b] Aragón Institute for Engineering Research, University of Zaragoza, IIS Aragón, Zaragoza, Spain
[c] CIBER in Bioengineering, Biomaterials and Nanomedicine (CIBER-BBN), Spain
[d] LaBS, Department of Chemistry, Materials and Chemical Engineering "Giulio Natta", Politecnico di Milano, Italy

ARTICLE INFO

Article history:
Received 9 May 2022
Revised 1 September 2022
Accepted 7 September 2022

Keywords:
Cardiac electrophysiological models
multi-scale simulations
stimulus current

ABSTRACT

Background and objective: In silico electrophysiological models are generally validated by comparing simulated results with experimental data. When dealing with single-cell and tissue scales simultaneously, as occurs frequently during model development and calibration, the effects of inter-cellular coupling should be considered to ensure the trustworthiness of model predictions. The hypothesis of this paper is that the cell-tissue mismatch can be reduced by incorporating the effects of conduction into the single-cell stimulation current. Methods: Five different stimulation waveforms were applied to the human ventricular O'Hara-Rudy cell model. The waveforms included the commonly used monophasic and biphasic (symmetric and asymmetric) pulses, a triangular waveform and a newly proposed asymmetric waveform (stimulation A) that resembles the transmembrane current associated with AP conduction in tissue. A comparison between single-cell and fiber simulated results was established by computing the relative difference between the values of AP-derived properties at different scales, and by evaluating the differences in the contributions of ionic conductances to each evaluated property. As a proof of the benefit, we investigated multi-scale differences in the simulation of the effects induced by dofetilide, a selective I_{Kr} blocker with high torsadogenic risk, on ventricular repolarization at different pacing rates. Results: Out of the five tested stimulation waveforms, stimulation A produced the closest correspondence between cell and tissue simulations in terms of AP properties at steady-state and under dynamic pacing and of ionic contributors to those AP properties. Also, stimulation A reproduced the effects of dofetilide better than the other alternative waveforms, mirroring the 'beat-skipping' behavior observed at fast pacing rates in experiments with human tissue. Conclusions: The proposed stimulation current waveform accounts for inter-cellular coupling effects by mimicking cell excitation during AP conduction. The proposed waveform improves the correspondence between simulation scales, which could improve the trustworthiness of single-cell simulations without adding computational cost.

1. Introduction

Computational models of cardiac electrophysiology provide an excellent tool to improve our understanding of the electrical activity of the heart. In particular, action potential (AP) models of cardiac myocytes can be used to understand cellular electrical function under physiological conditions or in response to disease or drug-induced alterations [1]. There are exciting opportunities for the adoption of cardiac models with predictive capacity, but these will require rigorous assessment of model credibility and prediction confidence [2].

Discrepancies between model outputs and the real system arise from different factors, including the necessary assumptions and simplifications embedded in a model, lack of knowledge, or differences between simulated and experimental conditions during the development of a model, among others. To increase the credibility of the model outputs, such factors should be reduced to the largest possible extent [3]. One way to do this is by replicating experimental conditions as closely as possible during model development and calibration [4].

* Corresponding author.
E-mail address: vmonasterio@usj.es (V. Monasterio).

https://doi.org/10.1016/j.cmpb.2022.107121

Cardiac electrophysiological models are often calibrated against experimental electrophysiological properties measured from patient samples, including AP duration (APD), maximum transmembrane potential, upstroke velocity or AP triangulation, among others [5]. Due to the susceptibility of some ion channels to cell isolation procedures [6,7], the reference experimental values for some of these properties may be obtained from small tissue preparations. In such cases, the resulting characterization of electrophysiological properties can be strongly influenced by inter-cellular coupling. Not accounting for coupling effects may inadvertently introduce a source of discrepancy when comparing cell simulation results with experimental observations, since not all AP-derived properties present a close correspondence between values measured in cells and in tissues [8]. Ideally, the cell-tissue discrepancies could be avoided by simulating the behavior of cardiac tissue for calibration. This approach, however, would greatly increase the computational cost of calibration and may, thus, not be suitable for studies requiring thousands of model simulations, such as those based on populations of models [5].

In situations where experimental data measured from tissue needs to be compared to simulation results from single cells (SCs), feasible alternatives to massive tissue simulations should try to incorporate, as much as possible, the effects of inter-cellular coupling into SC simulations. One way to achieve this is by defining the stimulation current to imitate cell excitation during AP conduction in tissue. Biphasic waveforms with square [9] and triangular [10] shapes have been proposed as alternatives to the commonly used monophasic stimulation pulses to excite SC models. Similarly, the effects of the shape, amplitude and timing of monophasic and biphasic square stimulation waveforms on AP generation have been evaluated in the context of cardiac defibrillation [11]. The scope of these works, however, does not include the evaluation of stimulation waveform effects on cell-tissue discrepancies.

In this work, we apply five alternative stimulation waveforms to the human ventricular O'Hara-Rudy model (ORd) [12] and quantify the mismatch between AP-derived properties measured in simulated cells and tissues. This comparison builds on a preliminary study [13] exploring the application of a symmetric axial-like current waveform to SCs simulated with the human ventricular ten Tusscher et al. model [14]. The present study includes, in addition to the usual monophasic pulse and the aforementioned biphasic square and triangular alternative waveforms, a new physiological-like asymmetric waveform that resembles the transmembrane current associated with AP conduction in tissue. The effect of each stimulation waveform on the relative contribution of ionic currents to the resulting AP properties and on the rate dependence of the APD is subsequently assessed. Finally, an example of application is provided to demonstrate the superiority of the physiological-like stimulation waveform for the study of the rapid delayed rectifying current, I_{Kr}, block-induced effects at fast pacing rates.

2. Methods

2.1. Computational simulations

The ORd model [12], one of the most widely used and extensively tested models of a human ventricular myocyte, was used to represent cellular electrophysiology. The endocardial version of the ORd model was employed unless otherwise stated. Following the authors' recommendation, we replaced the I_{Na} formulation with that from the ten Tusscher et al. model [14] to prevent propagation failure. The system of ordinary differential equations defining the cellular model was solved by using forward Euler integration with a time step of 0.002 ms.

For tissue simulations, we created a homogeneous 1-cm long fiber composed of endocardial cells. Electrical propagation across the cardiac tissue was modeled with the monodomain reaction-diffusion equation. Discretization was performed with a space step of 0.1 mm and a time step of 0.002 ms. The value of the conductivity was set to obtain a conduction velocity close to 65 cm/s under control conditions [15]. The first cell in the fiber was stimulated with monophasic current pulses with an amplitude of twice the diastolic threshold and a duration of 1 ms. The AP markers described in Sections 2.2 and 2.3 were computed as the mean value of the markers measured at three different positions within the cable located at: 0.25, 0.5, and 0.75 cm. The simulation software ELVIRA was used for the computations [16].

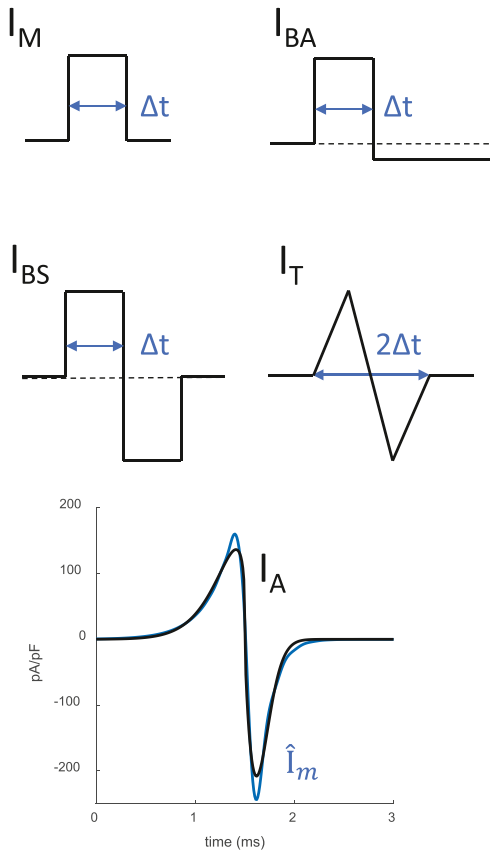

Fig. 1. Stimulus current waveforms for SC simulations. From top to bottom and left to right: monophasic (M), biphasic asymmetric (BA), biphasic symmetric (BS), triangular (T) and adjusted (A) waveforms. The adjusted stimulus current waveform (A) is shown with dark line, superposed to the reference current waveform extracted from 1D simulations $\hat{I}_m$ (light line).

We compared five waveforms for the stimulus current (Fig. 1) applied onto SCs:

1. Monophasic pulse (M) with a duration Δt and an amplitude of A pA/pF.
2. Biphasic asymmetric pulse (BA), defined as in [9]:

$$I_{BA}(t) = \begin{cases} A, & 0 \le t < \Delta t \\ \dfrac{-A\Delta t}{T - \Delta t}, & \Delta t \le t \le T \end{cases}$$

   where T is the pacing cycle length.
3. Biphasic symmetric pulse (BS), defined as:

$$I_{BS}(t) = \begin{cases} A, & 0 \le t < \Delta t \\ -A, & \Delta t \le t \le 2\Delta t \end{cases}$$

4. Triangular pulse (T), defined as:

$$I_T(t) = \begin{cases} mt, & 0 \le t < \frac{2\Delta t}{3} \\ -2m(t-\Delta t), & \frac{2\Delta t}{3} \le t < \frac{4\Delta t}{3} \\ m(t-2\Delta t) & \frac{4\Delta t}{3} < t \le 2\Delta t \end{cases}$$

with $m = 1.5A/\Delta t$.
For waveforms M, BS, BA and T, the amplitude A was set to twice the diastolic threshold and Δt was set to 1 ms.

5. The fifth alternative, denoted as Adjusted waveform (A), was designed to closely resemble axial current associated with the electrotonic coupling between myocytes. The adjusted waveform was built as the composition of two time-shifted and inverted Weibull curves:

$$I_A(t) = \begin{cases} A_l\left(\frac{\Delta t - t}{\alpha_l}\right)^{\beta_l - 1} \exp\left[-\left(\frac{\Delta t - t}{\alpha_l}\right)^{\beta_l}\right], & 0 \le t \le \Delta t \\ -A_r\left(\frac{t - \Delta t}{\alpha_r}\right)^{\beta_r - 1} \exp\left[-\left(\frac{t - \Delta t}{\alpha_r}\right)^{\beta_r}\right], & \Delta t < t < 2\Delta t. \end{cases}$$

The values of the parameters in the above equation were set by least-squares fitting the $I_A(t)$ equation to a reference waveform $\hat{I}_m$ taken as the transmembrane current of the central cell in the fiber for a control simulation. Those values were: $\alpha_l = 0.2942$ ms, $A_l = 236.8334$ pA/pF, $\beta_l = 1.2801$ ms, $\alpha_r = 0.1958$ ms, $A_r = 454.8173$ pA/pF, $\beta_r = 1.7160$ ms and $\Delta t = 1.5$ ms. As an additional analysis, the applicability of the adjusted stimulation, $I_A(t)$, to 2D or 3D simulations was explored by comparing the reference waveform $\hat{I}_m$ to the transmembrane current of a central cell in a 2D and 3D tissue (see details in Supplementary section S1.1).

2.2. Steady-state AP markers

2.2.1. AP markers under control conditions

Several AP measures were computed from fiber and SC simulations, including both depolarization and repolarization markers. In particular, we computed the APD at different percentages of repolarization (90%, 70%, 50%, 30%, and 10%), AP triangulation as $APD_{90} - APD_{30}$, the AP amplitude (APA), and the maximum AP slope (dV/dt_{max}). Control conditions were simulated by stimulating fiber and SC models for 150 cycles at 1 Hz and at 2 Hz. AP markers were calculated from the final paced beat of each simulation. A comparison between SC and fiber simulated results was established by computing the relative difference between the values of each marker m_j measured in SC (m_j^c) and in fiber (m_j^f) as:

$$E(\%) = \frac{m_j^c - m_j^f}{m_j^f} \cdot 100.$$

The applicability of the proposed stimulation to other cell types was explored by conducting the same comparison described above, now with the epicardial and mid-myocardial versions of the ORd model, with the atrial model by Courtemanche et al. [17], and with the Purkinje cell model by Stewart et al. [18] (see details in Supplementary section S1.2).

2.2.2. Ionic contributors to AP markers

The individual contribution of each major ionic conductance to modulation of AP markers was assessed next. Each conductance was varied by ± 15% and ± 30% and its role in determining each physiological AP-derived marker was evaluated by using a first order response surface model:

$$c_j \approx m_j + \sum_{i=1}^{N} \Delta_i \cdot w_{j,i}$$

where c_j is the value of the physiological marker j under the analyzed condition, m_j is the value of the marker j under control conditions, Δ_i is the variation of the ionic conductance relative to its control value, and the weight $w_{i,j}$ represents the contribution of the current i to the marker j. The contributions $w_{i,j}$ were estimated using the methodology developed in Carro et al. [8].

2.3. APD rate dependence

APD rate dependence was studied in SC and fiber simulations using a dynamic restitution protocol. Pacing started from 1 Hz with a train of 150 stimuli, and then the pacing frequency was incremented in steps of 0.1 Hz after each 150-beat train until a maximum frequency of 6 Hz. The steady-state APD_{90} of the last two cycles for each CL were recorded for analysis.

2.4. Simulated effects of dofetilide

To illustrate the potential benefits of the proposed physiological stimulation A, we investigated the effects of the drug dofetilide, a selective I_{Kr} blocker with high torsadogenic risk, on ventricular repolarization at different pacing rates. Previous studies in the literature [19] showed that simulated SC data, stimulated with non-physiological waveforms, were not in full agreement with experimental endocardial tissue data, and we tested the capacity of the physiological stimulation to overcome such issues.

We simulated the effect of a 0.1 μM dose of dofetilide as an 80.9% I_{Kr} block, following the methods in Britton et al. [19] based on the dataset by Kramer et al. [20]. We then compared the APs simulated with the endocardial SC model under BA and A stimulation to the APs of the fiber model. Simulations were performed by applying a train of 150 impulses at 1 Hz and then were repeated at 2 Hz.

Additionally, a supplementary analysis was performed to evaluate the effects of dofetilide on the generation of early afterdepolarizations (EADs) in mid-myocardial cells and tissue (see details in Supplementary section S1.3).

3. Results

3.1. Steady-state AP markers

3.1.1. AP markers under control conditions

At 1-Hz pacing under control conditions, stimulation A rendered results in SC that were very close to those measured in the fiber. For the ORd endocardial model, all markers presented improved performance under stimulation A as compared to the other stimulation waveforms (Table 1). In particular, stimulation A produced a substantial reduction in the differences between cell and fiber for APD_{10}, and dV/dt_{max}. Among the repolarization markers, the highest reduction was found for *Triangulation* (8.8% vs. -0.1% for M and A stimulation, respectively). Results at 2-Hz pacing confirmed the superiority of stimulation A over the alternatives. The results for the other models (Tables S2 to S5) also showed consistent improvement in the correspondence between SC and fiber markers for stimulation A.

3.1.2. Ionic contributions to AP markers

Ionic contributors to each AP marker are summarized in Fig. 2 when measured in fiber and when measured in SCs under different stimulation waveforms. As can be observed from the table, only stimulation A led to ionic mechanisms of AP markers in concordance with those obtained from fiber simulations.

Analysis of the role played by individual ionic conductances in modulating AP properties highlighted the benefits of using stimulation A. Variations in sodium conductance, G_{Na}, were found to affect all APD-based markers, Triangulation and *APA* when computed under stimulation waveforms M and BA. In contrast, none of those

Table 1
AP markers for fiber (F) and relative differences E(%) between markers in fiber and cell with stimulation M, BA, BS, T and A at 1 Hz (left) and 2-Hz pacing (right).

	1 Hz						2 Hz					
	F	M (%)	BA (%)	BS (%)	T (%)	A (%)	F	M (%)	BA (%)	BS (%)	T (%)	A (%)
APD_{90} (ms)	267.9	-1.5	-5.3	-0.8	-0.2	0.0	233.0	0.9	-6.0	1.0	1.6	-0.2
APD_{70} (ms)	241.3	-2.3	-6.0	-2.9	-1.3	0.0	207.1	0.2	-6.5	-1.0	0.8	-0.2
APD_{50} (ms)	209.7	-3.5	-7.1	-6.1	-3.0	0.0	177.4	-0.8	-7.2	-3.8	-0.4	-0.1
APD_{30} (ms)	171.5	-7.3	-10.8	-2.3	-2.0	0.1	145.2	-4.9	-11.0	-0.3	0.2	-0.1
APD_{10} (ms)	89.6	-29.1	-33.6	3.2	3.7	-0.7	84.0	-27.1	-35.7	-0.7	0.3	-0.8
APA (mV)	124.3	5.5	5.9	12.1	4.8	0.1	122.4	5.7	6.4	11.9	4.6	0.0
$dV/dt_{max}(V/s)$	241.9	37.5	33.9	68.7	55.1	-3.4	229.5	36.8	39.7	69.9	57.7	-5.9
Trian. (ms)	96.4	8.8	4.7	1.9	2.8	-0.1	87.8	10.4	2.3	3.1	3.9	-0.2

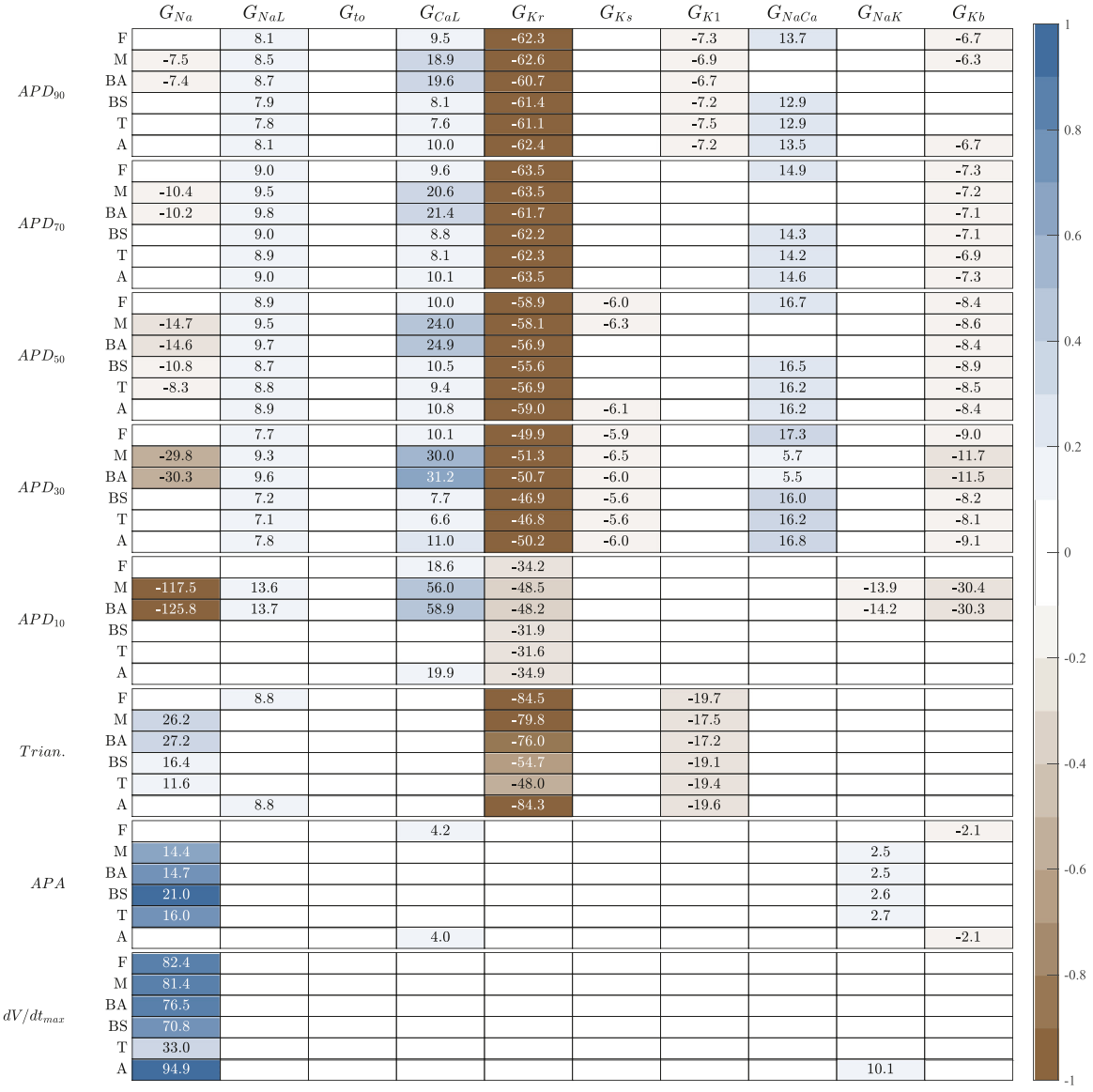

Fig. 2. Contribution of ionic conductances to AP markers simulated in fiber (F) and cell (stimulation M, BA, BS, T, and A). Percentages in boxes indicate the contribution of changes in a conductance to changes in a marker. For clarity, contributions lower than 1% and conductances with no influence on the selected markers are omitted in the representation. For each marker, the maximum absolute contribution among all conductances and stimulation options is indicated with the darkest color in the scale, and the rest of the contributions are colored according to their relative value with respect to the maximum.

markers were sensitive to G_{Na} variations in fiber simulations, a behavior that was closely replicated by SC simulations under stimulation A. Other noteworthy differences were found for conductances G_{CaL} and G_{NaCa}. In particular, G_{CaL} exerted a notably higher influence on APD markers for waveforms M and BA than for fiber and A simulations. Also, no influence of G_{CaL} was found for *APA* in M and BA simulations while positive correlation was found in fiber and A simulations. In the case of G_{NaCa}, the influence on APD markers was very low or zero for M and BA simulations while it was high in fiber and A simulations.

Out of the five stimulation waveforms tested in SC simulations, the relative contributions of ionic conductances were found to be

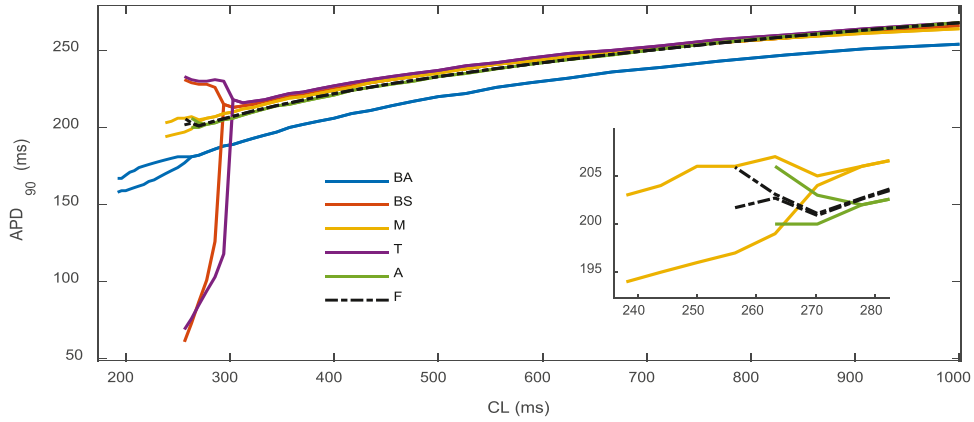

Fig. 3. APD_{90} rate dependence. Curves were generated with a dynamic pacing protocol. The inset graph to the right shows a zoom of the ending part of F, A and M curves.

very similar for M and BA waveforms, on the one hand, and for T and BS waveforms, on the other hand. Stimulation A differed from those four stimulation waveforms and was the one rendering the most similar results to those measured in fiber. Relevant differences between A and F results were found only in the case of the G_{NaK} influence on dV/dt_{max}.

In terms of the analyzed markers, the most notable differences were found for *APA*, where no common ionic contributors were found between fiber and SC simulations under M, BA, BS and T stimulation, being only stimulation A the one rendering sensitivity results similar to those in fiber. Similar observations apply to APD_{10}, even if to a lesser extent. For AP triangulation, G_{NaL} was found to be positively correlated with the marker under stimulation A and in fiber, whereas such contribution was attributed to G_{Na} under stimulation M, BS, BA and T.

3.2. APD rate dependence

As can be seen from the dynamic restitution curves (Fig. 3), AP alternans appeared in all SC and fiber simulations. However, while the magnitude of the alternating wave was found to be of low amplitude when measured under stimulation A and in the fiber, it was of much higher amplitude for all other stimulation waveforms. Also, the range of CLs associated with AP alternating behavior in the fiber was only reproduced under stimulation A but not under stimulation M, BA, BS and T.

The CL at which impulses failed to generate full APs was: 238 ms for M, 192 ms for BA, 265 ms for BS, 256 ms for T and 263 ms for A. In fiber, the CL at which conduction ceased to be stable was 256 ms.

3.3. Simulated effects of dofetilide

In SC and fiber paced at 1 Hz, simulation of dofetilide-induced I_{Kr} block led to substantial APD prolongation (Fig. 4). While APD prolonged by 95.7% in SC under BA stimulation, the prolongation was 105.2% in SC under A stimulation and 105.5% in fiber.

At 2-Hz pacing, SC simulations with BA stimulation caused 75.8% APD prolongation in all beats. On the contrary, in SC simulations with A stimulation and in fiber, APD was prolonged by 145.2% and 139.0%, respectively, only in half of the beats since APD prolongation caused "beat skipping" (see Fig. 4 bottom row, middle

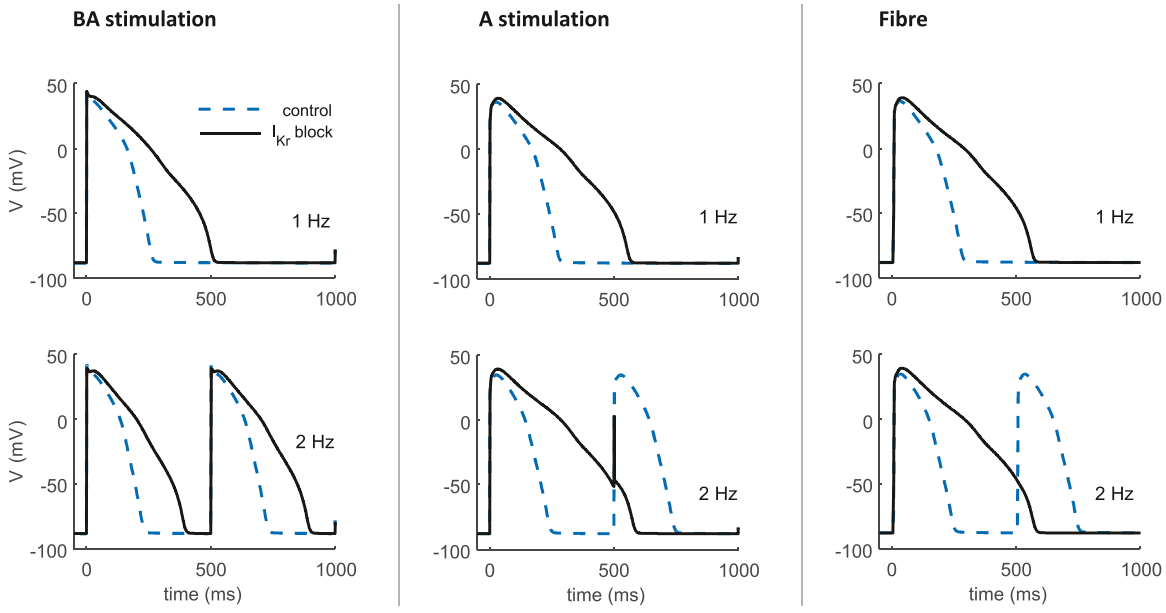

Fig. 4. Simulated effects of dofetilide on AP. Left: SC simulations with the BS stimulation; Middle: SC simulations with the A stimulation; Right: simulations in fiber. In all cases the blue traces correspond to control conditions and the black traces correspond to an I_{Kr} block of 80.9%. Top panels show simulations at 1 Hz and bottom panels at 2 Hz.

and right panels). This behavior is consistent with *ex vivo* experimental observations in human trabeculae [21], as reported in [19].

4. Discussion

We proposed a physiological-like waveform to stimulate SCs and reproduce tissue-like AP properties. Results in different simulation scenarios showed that the proposed waveform minimizes the discrepancy between SC and tissue AP properties, which can improve the credibility of model predictions when SC AP markers are to be compared with tissue-derived reference values.

The cell-tissue discrepancy has been acknowledged as a potential limitation of *in silico* studies [10,12,19,22,23], but the associated effects have not been systematically analyzed. A possible reason for this may be that differences between AP markers from SC and tissue simulations are relatively small in comparison to the range of experimental tissue measurements, particularly for repolarization markers. However, recent works discussing computational modeling reliability and credibility place strong emphasis on elucidating the sources of discrepancy between the outputs of *in silico* models and the systems they aim to describe [3,4]. In this sense, it is important that computational simulations represent the reality they are intended to model as closely as possible, so that the model behavior is a more trustworthy representation of the actual physiological processes in the real system.

In our study, a number of waveforms were compared for the stimulus current in SC simulations, with the goal of reproducing tissue electrophysiological characteristics. The physiological-like waveform proposed to mimic tissue behavior is based on the adjustment to a reference waveform extracted from simulations conducted in a fiber of homogeneous cells. The adjusted waveform reflects the source-sink behavior associated with AP propagation in tissue [24]. In SCs stimulated with the adjusted waveform, AP markers were most similar to those measured in fiber simulations. The adjusted stimulation also improved the match between the set of ionic conductances contributing to AP markers in SC and fiber simulations. These results suggest that the adapted stimulation can be a convenient alternative to the monophasic or biphasic asymmetric pulses when a population of models needs to be calibrated with or validated against experimental data from tissue preparations, specially in cases where AP amplitude or upstroke slope are used for evaluation.

Regarding APD rate dependence, fiber simulation results are consistent with experimental findings in healthy human tissue [25], where AP alternans with onset heart rates over 200 beats per minute and narrow CL ranges were observed. The adjusted waveform produced the most similar behavior to fiber simulations, possibly due to the reduced mismatch in G_{CaL} and G_{NaCa}, since I_{CaL} and I_{NaCa} are hypothesized to play a major role in the generation of AP alternans [26]. In studies where the output of cell models needs to be compared with experimental measures in cardiac tissues to unravel the mechanisms of alternans, it might be worth considering whether the mismatch between scales could be introducing unwanted discrepancy. Our results suggest that the adjusted stimulation waveform will reproduce experimental data in tissue more accurately, which will make the attribution of the observed phenomena to underlying physiological mechanisms more credible.

Our proposed methodology represents a cost-effective way of reproducing experimental tissue data in *in silico* SC studies. The stimulus waveform derived from the 1D simulation (which needs to be performed only once) can be applied to study a variety of conditions, such as different pacing frequencies and changes in ionic current conductances due to drug-induced current blocks, without the need to perform all these simulations in a fiber. Our results illustrate this advantage, with only one reference fiber simulation being sufficient to approximate the AP characteristics in tissue in all the analyzed scenarios. Furthermore, the strong similarity between the transmembrane current waveforms estimated from 1D, 2D and 3D tissues (Figure S1) suggests that the adjusted stimulus could also be applicable to studies involving measurements in 2D or 3D homogeneous tissues. In practice, it is necessary to point out that the adjusted waveform depends on the model-specific AP morphology. To facilitate the application to other models, adjusted waveform parameters are readily provided for the epicardial and mid-myocardial ORd model, the Stewart et al. Purkinje model [18] and the Courtemanche et al. atrial model [17] (Table S1).

To illustrate the potential benefits of the physiological-like adjusted stimulation, we investigated the effects of the selective I_{Kr} blocker dofetilide at different pacing rates. Our results suggest that the adjusted waveform could be useful for the analysis of inter-individual variability in drug response, in cases where a population of models needs to be calibrated with experimental data from homogeneous tissues. In those situations, the output of the models could be reflecting not only the physiological mechanisms under study, but also the undesired effects of scale discrepancy. Our results on the effect of dofetilide with the baseline ORd model demonstrate that the scale discrepancy effects can be minimized by using the adjusted stimulation. In our example, the skipping behavior observed at 2 Hz for simulated fibers and SCs stimulated with waveform A was consistent with experimental observations [27] as reported in [19]. The mismatch between experimental tissue results and SC results stimulated with waveform BA found in our study was already observed in [19], and was suggested to arise from differences in the stimulation current. Our results support that interpretation and demonstrate a way of increasing the trustworthiness of *in silico* predictions involving different scales.

In this work, the proposed waveform is intended to approximate the AP characteristics in homogeneous tissue. Additional uses could include the use of the physiological-like stimulus in experimental settings involving clamp techniques. Possible extensions of the study could involve the parameterization of the physiological-like stimulus from experimental data for its use in current or dynamic clamp experiments [28].

5. Conclusion

A novel physiological-like stimulation waveform resembling the transmembrane current associated with AP conduction in tissue has been proposed as a cost-effective way to approximate the AP characteristics in simulated tissue. The proposed waveform is compared to other common biphasic and monophasic forms of stimulation and is found to produce the best correspondence between AP-derived markers in SC and fiber simulations and the most similar ionic contributors to AP properties. Additionally, comparison to experimental observations on the effects of dofetilide indicate that the proposed stimulus can narrow the gap between SC simulations and tissue experimental observations.

Declaration of Competing Interest

The authors declare that they have no known competing financial interests or personal relationships that could have appeared to influence the work reported in this paper.

Acknowledgement

This work was supported by Ministerio de Ciencia e Innovación (Spain) through project PID2019-105674RB-I00 and by Aragón Government through BSICoS group (T39_20R) and projects LMP94_21 and LMP141_21 from Departamento de Ciencia, Universidad y Sociedad del Conocimiento. Computations were carried out in DENIS

(Volunteer Computer platform supported by Universidad San Jorge through Proyecto Interno CoMBA 2021-22).

Supplementary material

Supplementary material associated with this article can be found, in the online version, at doi:10.1016/j.cmpb.2022.107121

References

[1] S.A. Niederer, J. Lumens, N.A. Trayanova, Computational models in cardiology, Nature Reviews Cardiology 16 (2) (2019) 100–111, doi:10.1038/s41569-018-0104-y.

[2] G.R. Mirams, P. Pathmanathan, R.A. Gray, P. Challenor, R.H. Clayton, Uncertainty and variability in computational and mathematical models of cardiac physiology, Journal of Physiology 594 (23) (2016) 6833–6847, doi:10.1113/JP271671.

[3] R.H. Clayton, Y. Aboelkassem, C.D. Cantwell, C. Corrado, T. Delhaas, W. Huberts, C.L. Lei, H. Ni, A.V. Panfilov, C. Roney, R.W. Dos Santos, An audit of uncertainty in multi-scale cardiac electrophysiology models: Uncertainty Audit of Cardiac Models, Philosophical Transactions of the Royal Society A: Mathematical, Physical and Engineering Sciences 378 (2173) (2020), doi:10.1098/rsta.2019.0335.

[4] D.G. Whittaker, M. Clerx, C.L. Lei, D.J. Christini, G.R. Mirams, Calibration of ionic and cellular cardiac electrophysiology models, Wiley Interdisciplinary Reviews: Systems Biology and Medicine, 10.1161 12 (4) (2020) 1–42.

[5] A. Muszkiewicz, O.J. Britton, P. Gemmell, E. Passini, C. Snchez, X. Zhou, A. Carusi, T.A. Quinn, K. Burrage, A. Bueno-Orovio, B. Rodriguez, Variability in cardiac electrophysiology: Using experimentally-calibrated populations of models to move beyond the single virtual physiological human paradigm, Prog Biophys Mol Biol 120 (1-3) (2016) 115–127, doi:10.1016/j.pbiomolbio.2015.12.002.

[6] S. Rajamani, C.L. Anderson, C.R. Valdivia, L.L. Eckhardt, J.D. Foell, G.A. Robertson, T.J. Kamp, J.C. Makielski, B.D. Anson, C.T. January, Specific serine proteases selectively damage KCNH2 (hERG1) potassium channels and I(Kr), American Journal of Physiology-Heart and Circulatory Physiology 290 (3) (2006) H1278–H1288.

[7] L. Yue, J. Feng, G. Li, S. Nattel, Transient outward and delayed rectifier currents in canine atrium: properties and role of isolation methods, American Journal of Physiology-Heart and Circulatory Physiology 270 (6) (1996) H2157–H2168.

[8] J. Carro, J.F. Rodrguez-Matas, V. Monasterio, E. Pueyo, Limitations in electrophysiological model development and validation caused by differences between simulations and experimental protocols, Prog Biophys Mol Biol 129 (2017) 53–64, doi:10.1016/j.pbiomolbio.2016.11.006.

[9] L. Livshitz, Y. Rudy, Uniqueness and stability of action potential models during rest, pacing, and conduction using problem-solving environment, Biophys J 97 (5) (2009) 1265–1276, doi:10.1016/j.bpj.2009.05.062.

[10] Z. Syed, E. Vigmond, S. Nattel, L.J. Leon, Atrial cell action potential parameter fitting using genetic algorithms, Medical & Biological Engineering & Computing 43 (5) (2005) 561–571, doi:10.1007/BF02351029.

[11] L.J. Leon, F.A. Roberge, A Model Study of Extracellular Stimulation of Cardiac Cells, IEEE Transactions on Biomedical Engineering 40 (12) (1993) 1307–1319, doi:10.1109/10.250586.

[12] T. O'Hara, L. Virág, A. Varró, Y. Rudy, Simulation of the undiseased human cardiac ventricular action potential: Model formulation and experimental validation, PLoS Computational Biology 7 (5) (2011), doi:10.1371/journal.pcbi.1002061.

[13] V. Monasterio, E. Pueyo, J. Rodríguez-Matas, J. Carro, Influence of the stimulation current on the differences between cell and tissue electrophysiological simulations, in: 2019 Computing in Cardiology (CinC), IEEE, 2019, pp. 1–4.

[14] K.H.W.J. ten Tusscher, V.a. Panfilov, Alternans and spiral breakup in a human ventricular tissue model, Am J Physiol Heart Circ Physiol 291 (3) (2006) H1088–H1100, doi:10.1152/ajpheart.00109.2006.

[15] P. Taggart, P.M. Sutton, T. Opthof, R. Coronel, R. Trimlett, W. Pugsley, P. Kallis, Inhomogeneous transmural conduction during early ischaemia in patients with coronary artery disease, J Mol Cell Cardiol 32 (4) (2000) 621–630, doi:10.1006/jmcc.2000.1105.

[16] E.a. Heidenreich, J.M. Ferrero, M. Doblaré, J.F. Rodríguez, Adaptive macro finite elements for the numerical solution of monodomain equations in cardiac electrophysiology, Ann Biomed Eng 38 (7) (2010) 2331–2345, doi:10.1007/s10439-010-9997-2.

[17] M. Courtemanche, R.J. Ramirez, S. Nattel, Ionic mechanisms underlying human atrial action potential properties: insights from a mathematical model, American Journal of Physiology-Heart and Circulatory Physiology 275 (1998) H301–H321.

[18] P. Stewart, O.V. Aslanidi, D. Noble, P.J. Noble, M.R. Boyett, H. Zhang, Mathematical models of the electrical action potential of purkinje fibre cells, Philosophical transactions. Series A, Mathematical, physical, and engineering sciences 367 (2009) 2225–2255, doi:10.1098/rsta.2008.0283.

[19] O.J. Britton, N. Abi-Gerges, G. Page, A. Ghetti, P.E. Miller, B. Rodriguez, Quantitative comparison of effects of dofetilide, sotalol, quinidine, and verapamil between human ex vivo trabeculae and in silico ventricular models incorporating inter-individual action potential variability, Frontiers in Physiology 8 (AUG) (2017) 1–19, doi:10.3389/fphys.2017.00597.

[20] J. Kramer, C.A. Obejero-Paz, G. Myatt, Y.A. Kuryshev, A. Bruening-Wright, J.S. Verducci, A.M. Brown, Mice models: superior to the hERG model in predicting torsade de pointes, Scientific reports 3 (1) (2013) 1–7.

[21] G. Page, P. Ratchada, Y. Miron, G. Steiner, A. Ghetti, P.E. Miller, J.A. Reynolds, K. Wang, A. Greiter-Wilke, L. Polonchuk, et al., Human ex-vivo action potential model for pro-arrhythmia risk assessment, Journal of pharmacological and toxicological methods 81 (2016) 183–195.

[22] P. Gemmell, K. Burrage, B. Rodríguez, T.A. Quinn, Rabbit-specific computational modelling of ventricular cell electrophysiology: Using populations of models to explore variability in the response to ischemia, Progress in Biophysics and Molecular Biology 121 (2) (2016) 169–184.

[23] M. Paci, E. Passini, A. Klimas, S. Severi, J. Hyttinen, B. Rodriguez, E. Entcheva, All-Optical Electrophysiology Refines Populations of In Silico Human iPSC-CMs for Drug Evaluation, Biophysical Journal 118 (10) (2020) 2596–2611, doi:10.1016/j.bpj.2020.03.018.

[24] R.A. Gray, D.N. Mashburn, V.Y. Sidorov, J.P. Wikswo, Quantification of transmembrane currents during action potential propagation in the heart, Biophys J 104 (1) (2013) 268–278, doi:10.1016/j.bpj.2012.11.007.

[25] M.L. Koller, S.K. Maier, A.R. Gelzer, W.R. Bauer, M. Meesmann, R.F. Gilmour, Altered dynamics of action potential restitution and alternans in humans with structural heart disease, Circulation 112 (11) (2005) 1542–1548, doi:10.1161/CIRCULATIONAHA.104.502831.

[26] T. You, C. Luo, K. Zhang, H. Zhang, M.A. Colman, Electrophysiological Mechanisms Underlying T-Wave Alternans and Their Role in Arrhythmogenesis, Frontiers in physiology 12 (March) (2021), doi:10.3389/fphys.2021.614946.

[27] G. Page, P. Ratchada, Y. Miron, G. Steiner, A. Ghetti, P.E. Miller, J.A. Reynolds, K. Wang, A. Greiter-Wilke, L. Polonchuk, M. Traebert, G.A. Gintant, N. Abi-Gerges, Human ex-vivo action potential model for pro-arrhythmia risk assessment, Journal of Pharmacological and Toxicological Methods 81 (4) (2016) 183–195, doi:10.1016/j.vascn.2016.05.016.

[28] R. Wilders, Dynamic clamp: A powerful tool in cardiac electrophysiology, Journal of Physiology 576 (2006) 349–359, doi:10.1113/jphysiol.2006.115840.